Mirrorless lasing from light emitters in percolating clusters

Gennadiy Burlak[1,2] and Y. G. Rubo[1]

[1]*Instituto de Energías Renovables, Universidad Nacional Autónoma de México, Temixco, Morelos 62580, Mexico*

[2]*CIICAp, Universidad Autónoma del Estado de Morelos, Avenida Universidad 1001, Cuernavaca, Morelos 62210, Mexico*

(Received 22 April 2015; revised manuscript received 28 May 2015; published 8 July 2015)

We describe the lasing effect in the three-dimensional percolation system, where the percolating cluster is filled by active media composed by light emitters excited noncoherently. We show that, due to the presence of a topologically nontrivial photonic structure, the stimulated emission is modified with respect to both conventional and random lasers. The time dynamics and spectra of the lasing output are studied numerically with finite-difference time-domain approach. The Fermat principle and Monte Carlo approach are applied to characterize the optimal optical path and interconnection between the radiating emitters. The spatial structure of the laser mode is found by a long-time FDTD simulation.

DOI: 10.1103/PhysRevA.92.013812 PACS number(s): 42.55.Ah, 42.55.Zz, 78.67.−n, 42.70.Hj

I. INTRODUCTION

Recent development of micro- and nanophotonics demonstrated how intrinsic disorder in photonic materials can be exploited to create useful optical structures. One example is the random laser structures [1,2], in which the laser action is obtained in disordered media such as powders and porous glasses. The optical emitters (e.g., quantum dots) in inhomogeneous structures are interconnected radiatively which results in the field correlations and leads to various collective phenomena (see, e.g., [3,4] and references therein). The importance of interplay between light diffusion in random media and light amplification was demonstrated by Letokhov [5], and the interesting properties of mirrorless laser systems are widely studied since then, both experimentally [6–10] and theoretically [11–14] (see also the review [15]). In most random lasing materials, the intensity is spread throughout the sample and, in general, there are several lasing modes. In certain cases interference of different modes can lead to light localization [16–18], which is the optical counterpart of Anderson localization for electrons in disordered conductors. This can be understood in terms of the formation of randomly shaped nonoverlapping modes with exponentially large lifetimes [15]. Random lasing is also observed in photonic crystals with structural disorder, where the photonic band gap is progressively filled by the tails of resonances at its edges. There are experimental evidences of three-dimensional (3D) Anderson localization of light inside the gap [19].

The drawback of random lasers is that a great part of the excitation power is wasted, and lasing is additionally distributed among several lasing modes having distinct frequencies, placed in different parts of the sample, and shining light in different directions. One possibility to obtain better control on the laser emission is to achieve mirrorless lasing effect in some specially prepared irregular medium. A promising candidate of such a system is light emitters incorporated into 3D percolating clusters in solids [20–22] (see [23,24] for a review of percolation phenomena). At a small concentration of voids in such a system the number of clusters is insignificant. However, if the concentration of voids exceeds a certain threshold value, then a spanning (infinite) cluster is formed, and it penetrates the entire volume. This cluster produces global percolation in the system and qualitatively changes its properties. In particular, the laser effect in a percolating medium is expected to be noticeably different from the random laser phenomenon in conventional ("uniformly porous") materials. In the simplest way, it can be argued that already in a vicinity of the percolating phase transition the fractal dimension of the system $D_H \simeq 2.54$ considerably differs from the dimension of the embedded space $D = 3$. One of the important questions here is whether the mirrorless lasing effect can still be observed for a noninteger dimension case with a fractal (Hausdorff) dimension of $D_H < 3$, where one expects strong randomness of the properties of the system.

First we indicate the fundamental difference of lasing in percolating medium, as compared to the random lasing in conventional configuration. In the case of the standard random laser, the randomly distributed emitters are incorporated homogeneously in entire medium (see [15,19] and references therein). In contrast, in the system considered in this paper the emitters are integrated only into the percolating cluster having random complicated shape with noninteger fractal dimension. As a result, this system is strongly spatially nonuniform, and this leads to considerable multiply scattering and amplification of optical waves from the inhomogeneous random cluster structure. It is important to note that the diffusion approach is oversimplified to correctly describe the light amplification in the case of photon propagation in a scattering medium with nonuniformly distributed gain [25]. Therefore, we use the full-vectorial Maxwell-Bloch equations based on finite-difference time-domain (FDTD) technique instead of the diffusion approach.

To address these questions we study the spanning cluster in 3D embedded percolation environment as an object with a fractional dimension. Already the presence of incipient spanning cluster makes the system anisotropic and provides the connection between the input (on the high porosity side) and output (on the low porosity side); see Fig. 1. This also makes feasible the incorporation of emitters inside the cluster. Forcing the emitters ensemble through such a percolation medium allows creating a network of emitters, leaving other parts of the system unchanged. Here we investigate the lasing effect in this percolating spanning cluster, assuming the emitters are uniformly incorporated in it. Thus in this paper we describe a different type of mirrorless lasing, percolating lasing, that is a logical extension of previous works for case of random lasing that cannot be simplified to the standard laser case.

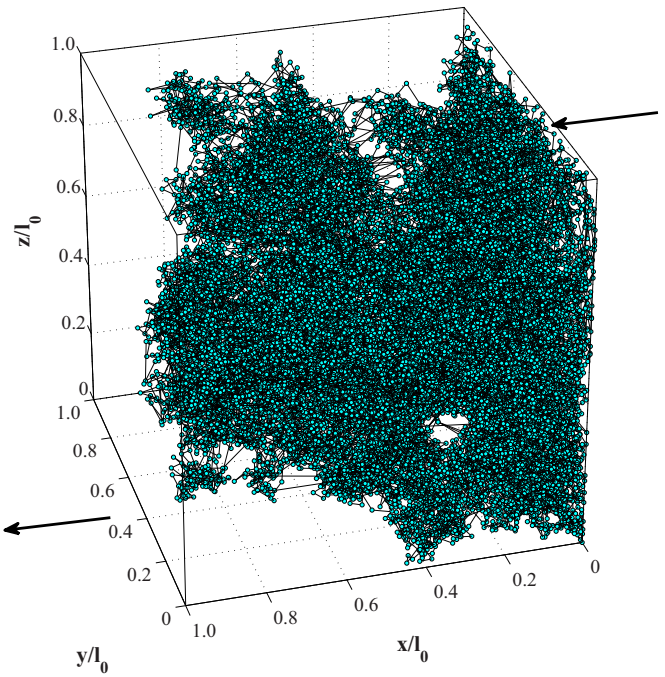

FIG. 1. (Color online) Typical spatial structure of the incipient percolating cluster near the percolation threshold at $p = 0.32$ in the cube $l_0 \times l_0 \times l_0$, where $l_0 = 10^{-4}$ m. The cluster is shown for $75 \times 75 \times 75$ numerical grid. Only sites coupled to the spanning cluster are shown, while all the internal sites unconnected to the entry side are not displayed. In this configuration a considerable quantity of the emitters are incorporated closely to the entry side (indicated by incoming arrow) of the crystal. The solid line connects the nodes joined with the use of the variational Fermat principle (see Sec. IV for details).

The paper is organized as follows. In Sec. II we formulate the main equations. In Sec. III we present the numerical results on the lasing emission from the emitters in percolating medium. Section IV contains the application of the Fermat principle to find the spatial interconnection between the emitters in this percolating system, and the last section contains conclusions.

II. BASIC EQUATIONS

We are interested in integral emission of electromagnetic energy from a cubical sample $(x,y,z) \in [0,l_0]$. The output flux of energy can be written as

$$I = \oint_S (\mathbf{K} \cdot \mathbf{n}) dS = I_x + I_y + I_z, \tag{1}$$

where $\mathbf{K}$ is the Pointing vector, $\mathbf{n}$ is the normal unit vector to the surface S of the cube, and $I_{x,y,z}$ indicate the fluxes from two faces of the cube perpendicular to a particular direction.

To find the emission from the system we solve numerically the equation coupling the polarization density $\mathbf{P}$, the electric field $\mathbf{E}$, and the occupations of the levels of emitters. In the case of uncoupled emitters this equation is [26]

$$\frac{\partial^2 \mathbf{P}}{\partial t^2} + \Delta\omega_a \frac{\partial \mathbf{P}}{\partial t} + \omega_a^2 \mathbf{P} = \frac{6\pi\varepsilon_0 c^3}{\tau_{21}\omega_a^2}(N_1 - N_2)\mathbf{E}. \tag{2}$$

Here $\Delta\omega_a = \tau_{21}^{-1} + 2T_2^{-1}$, where T_2 is the mean time between dephasing events, τ_{21} is the decay time from the second atomic level to the first one, and ω_a is the frequency of radiation. The electric and magnetic fields, $\mathbf{E}$ and $\mathbf{H}$, and the current $\mathbf{j} = \partial\mathbf{P}/\partial t$ are found from the Maxwell equations, together with the equations for the densities $N_i(\mathbf{r},t)$ of atoms residing in the ith level. In the case of four level laser, $i = 0,1,2,3$ and these rate equations read (see [27] and references therein)

$$\frac{\partial N_3}{\partial t} = A_r N_0 - \frac{N_3}{\tau_{32}}, \tag{3a}$$

$$\frac{\partial N_2}{\partial t} = \frac{N_3(t)}{\tau_{32}} + \frac{(\mathbf{j}\cdot\mathbf{E})}{\hbar\omega_a} - \frac{N_2}{\tau_{21}}, \tag{3b}$$

$$\frac{\partial N_1}{\partial t} = \frac{N_2(t)}{\tau_{21}} - \frac{(\mathbf{j}\cdot\mathbf{E})}{\hbar\omega_a} - \frac{N_1}{\tau_{10}}, \tag{3c}$$

$$\frac{\partial N_0}{\partial t} = \frac{N_1}{\tau_{10}} - A_r N_0. \tag{3d}$$

An external source excites emitters from the ground level ($i = 0$) to third level at a certain rate A_r, which is proportional to the pumping intensity in experiments. After a short lifetime τ_{32}, the emitters transfer nonradiatively to the second level. The second level and the first level are the upper and the lower lasing levels, respectively. Emitters can decay from the upper to the lower level by both spontaneous and stimulated emission, and $(\mathbf{j}\cdot\mathbf{E})/\hbar\omega_a$ is the stimulated radiation rate. Finally, emitters can decay nonradiatively from the first level back to the ground level. The lifetimes and energies of upper and lower lasing levels are τ_{21}, E_2, and τ_{10}, E_1, respectively. The individual frequency of the radiation of each emitter is then $\omega_a = (E_2 - E_1)/\hbar$.

To simulate the laser medium we consider the situation when the incipient percolating cluster is completely filled with light sources. Such a percolating cluster is shown in Fig. 1, where all internal uncoupled sites have been omitted. We indicate that the percolation cluster in Fig. 1 has a typical dendrite shape that, however, depends on the actual random sampling. Rerunning the simulation with another random seed value will lead to a percolation cluster with somewhat different geometry, which will also have a similar sponge structure. The cluster is grown in the x direction indicated by the arrow in Fig. 1, which provides a substantially asymmetric structure. Equations (1)–(3) are solved with initial conditions that correspond to inversion of occupations of the emitters levels and some random seed for the electromagnetic field that simulates the noise in the system [26,28].

III. NUMERICAL CALCULATIONS

The theory of lasing from disordered three-dimensional (3D) active media relies strongly on the huge amount of computational resources needed when dealing with 3D problems. The simpler, low-dimensional models (1D and 2D) are quite unsatisfactory for many important reasons, including the critical nature of the random lasing in three dimensions [19]. Since the classical diffusion model does not correctly describe the propagation of photons in a scattering medium with nonuniformly distributed gain or loss [25], we apply the FDTD technique for our numerical simulations. Briefly, the strategy

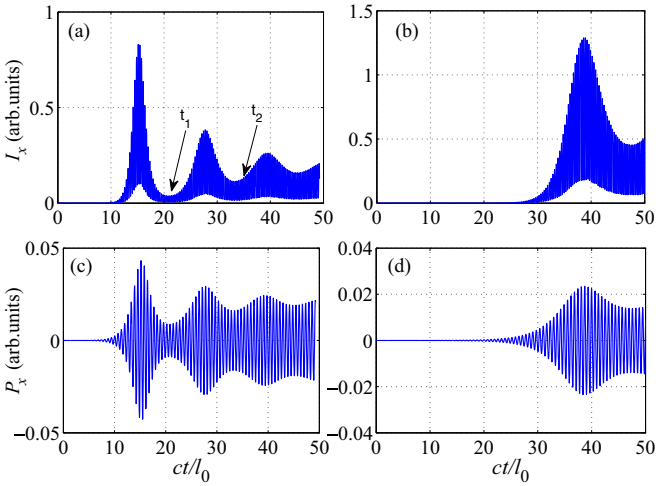

FIG. 2. (Color online) Showing the formation of laser generation. Panels (a) and (b) demonstrate the flux I_x in the x direction of the system; see (1). Panels (c) and (d) show the polarization $P_x(t)$ of the deepest emitting node in the cluster. In panels (a) and (c) the numerical grid with $L = 75$ has been used, while $L = 100$ in panels (b) and (d). The lasing start times are $t_s = 12l_0/c = 4$ ps and $t_s = 28l_0/c = 9.3$ ps for $L = 75$ and 100, respectively.

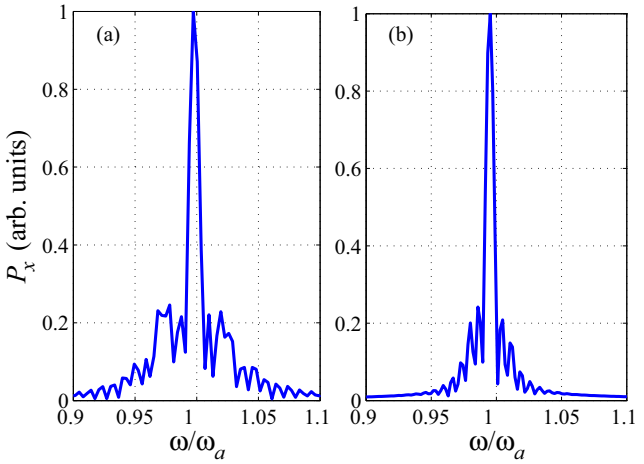

FIG. 3. (Color online) The spectral structure of field shown in Fig. 2. Panels (a) and (b) show the amplitudes of emission spectra for cases $L = 75$ and $L = 100$, respectively; panels (c) and (d) display the phases. An overall narrowing of the frequency spectrum is observed.

of our simulations consists in the following: (i) calculating the geometry of the spanning percolating cluster, (ii) calculating the photon field **E** generated by emitters incorporated in spanning cluster with the use of FDTD technique [20,29], and (iii) solution of nonlinear dynamic coupled equations for field, polarization **P**, and the occupation numbers N_i for all the emitters in the 3D system. The Runge-Kutta algorithm with automatic control of the time stepping has been applied for the latter.

In calculations we considered the gain medium with parameters close to GaN powder, similar to Ref. [6]. The lasing frequency ω_a is $2\pi \times 3 \times 10^{13}$ Hz, the lifetimes are $\tau_{32} = 0.3$ ps, $\tau_{10} = 1.6$ ps, $\tau_{21} = 16.6$ ps, and the dephasing time is $T_2 = 0.0218$ ps. The percolating cluster has been generated inside the cube of the $l_0 = 1$ μm edge having L^3 nodes, with $L = 75$ and $L = 100$ that was sufficient to simulate the percolating structure [20,21]. Each node is supposed to indicate the position of many emitters, with the total concentration of emitters inside the percolation cluster being $N_t = N_0 + N_1 + N_2 + N_3 = 3.3 \times 10^{24}$ m^{-3}. The initial (at $t = 0$) values of densities $N_0(0) = 0.001N_t$, $N_1(0) = 0.002N_t$, $N_1(0) = 0.002N_t$, and $N_3(0) = 0.995N_t$ are used. The refractive index of a host material is $n = 2.2$ that is close to the typical values for ceramics $Lu_3Al_5O_{12}$, $SrTiO_3$, ZrO_2; see review [30]. The results of simulations shown in Figs. 2–7 are obtained for cw pumping given by $A_r = 10^7$ s^{-1}. At this pumping all the simulations show the formation of a well-defined lasing for $t > t_s$, and we refer to t_s as the lasing start time in what follows. To simulate the noise in our system the initial seed for the electromagnetic field has been created with random phases at each node.

Figure 2 displays the dynamics of field and polarization as functions of time for emitters incorporated in a percolating cluster with occupation probability $p = 0.32$ in a simple cubic lattice, which is close to the critical percolation value $p_c \approx 0.3116$ (see Ref. [31]). Panels (a) and (b) show the flux of energy I_x in the growth direction [see Eq. (1)], while panels (c) and (d) display the polarizations $P_x(t)$ corresponding to the deepest (with respect of the entry surface) emitter in the percolating cluster. Comparing Figs. 2(a) and 2(b) we observe that the lasing start time t_s increases with the system size (L^3), or more precisely with the number of emitters incorporated in the cluster. This is due to the fact that an increase of the system size increases the volume of the phase synchronization (number of emitters) in a percolating medium. Figure 2 shows that the lasing begins with the spiking oscillations having

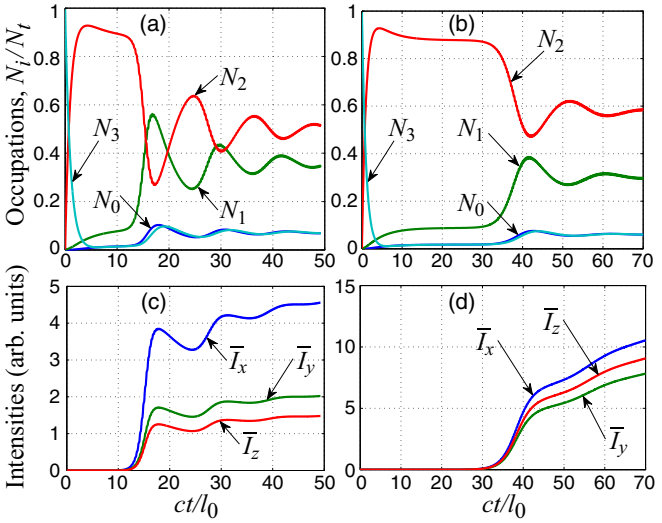

FIG. 4. (Color online) (a),(b) Dynamics of population numbers N_i ($i = 0,1,2,3$), where $N_{1,2}$ correspond to the lasing levels. The times $t_{1,2}$ of minima of the field output in Fig. 2(a) correspond to the intersections of lasing levels. (c),(d) Integrated over the observation time t intensities $\bar{I}_{x,y,z}$ of radiation emitted along corresponding directions. See details in text.

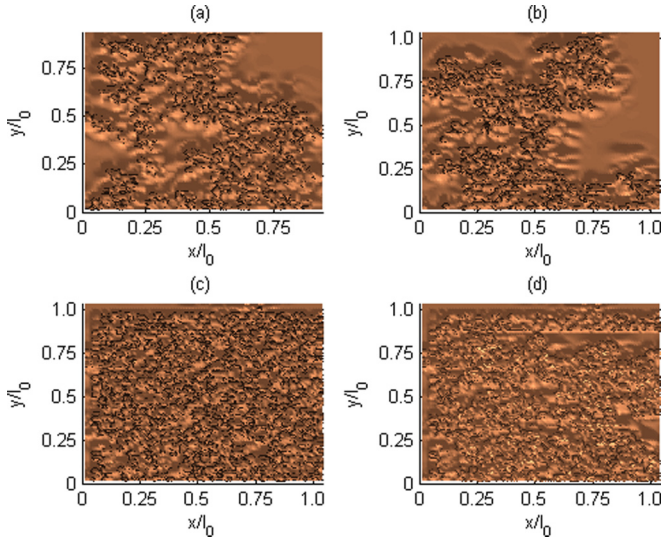

FIG. 5. (Color online) Finite-difference time-domain calculation of the spatial distribution of the field intensity (in central intersection of sample) in 3D percolating cluster for different system sizes with (a) $L = 75$, (b) $L = 83$, (c) $L = 82$, and (d) $L = 80$.

strongly modulated shape, but after some time the amplitude of oscillations decreases. Note that the phenomenon of "laser spiking" shown in Fig. 2 has being observed at fast turn-on of some lasers [32]. Normally such oscillations occur when the gain changes rapidly due to the fluctuations of pumping. In our case, however, such oscillations appear due to the considerably inhomogeneous distribution of emitters in the percolating medium. The other important feature of lasing from the percolating media is that the energy flux at output side $I_x(L)$ it is about twice more than the flux at input side $I_x(0)$ indicated by the incoming arrow in Fig. 1. The total emission along the growth direction is also more than twice stronger than the emission from the lateral sides. The presence of considerable directionality emission is presumably due to the substantial anisotropy of the incipient percolation cluster seen in Fig. 1.

To study the details of this lasing we investigated the spectra of the field output. Figure 3 displays the spectral structure of the output shown in Fig. 2 in panels (a) and (b) for $L = 75$ and $L = 100$, respectively. From Fig. 3 we observe that the spectrum has a rather indented shape beyond the central line. Note that this line is placed closely to the single emitter frequency ω_a but does not coincide with it exactly, and it shows substantial narrowing of the emission spectrum. The shift in the emission frequency appears because the surrounding media, in which the percolating cluster resides, serves as an effective cavity helping to keep the radiation inside the cluster and to form the lasing effect. As a result, at larger times after the excitation start, $t \gg t_s$, a great number of emitters become synchronized to contribute to the stimulating radiation. Contrary to the distributed random lasers, we observe that only one mode dominates at large times and this mode extends through the whole light emitted media, while all other modes are suppressed.

Figures 4(a) and 4(b) exhibit the dynamics of population numbers N_i (for the deepest emitter), where the levels 1 and 2

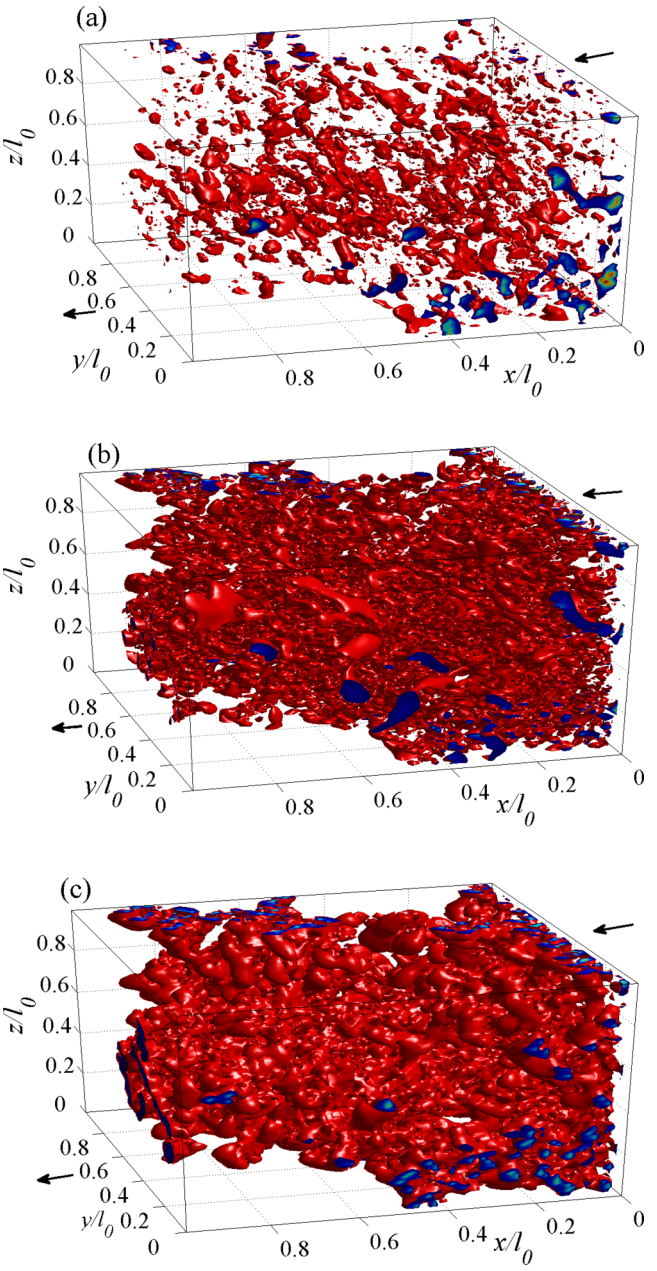

FIG. 6. (Color online) The FDTD simulations of 3D spatial structure of the field amplitude $|E_x|$, generated by emitters incorporated in percolating cluster (a) below the lasing regime, (b) at the lasing start time t_s, and (c) for well-developed lasing.

correspond to the laser levels. The emission intensity averaged over the total observation time, $\bar{I}_i(t) = t^{-1}\int_0^t I_i(\tau)d\tau$, is shown in Figs. 4(c) and 4(d), again for the cases $L = 75$ and $L = 100$, respectively. The fluxes of the emission energy through the growth direction $\bar{I}_x$ and the lateral sides $\bar{I}_{y,z}$ demonstrate considerably anisotropic emission at least in the considered case of the incipient percolating cluster.

Figure 5 shows the details of the finite-difference time-domain (FDTD) calculation of the distribution of the field intensity in the central intersection of the 3D sample in a spanning percolating cluster for systems of different sizes. One can observe fluctuating, nonuniform, and likely speckle

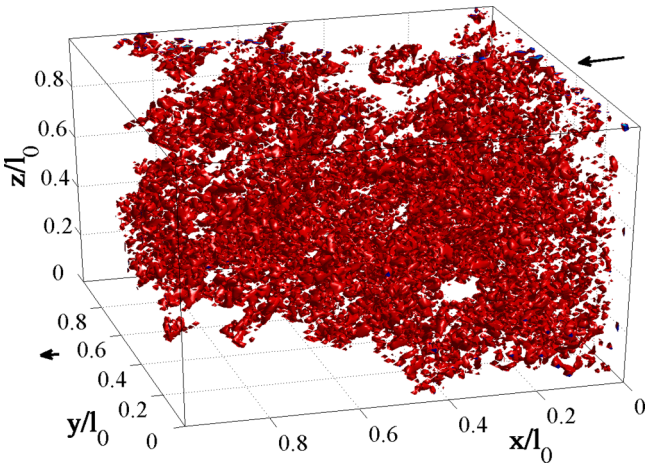

FIG. 7. (Color online) Dominant laser mode that is formed in the system with a long-time FDTD simulation. Comparison the shape of this mode to the Fermat optical path displayed in Fig. 1 shows reasonably good agreement of Fermat path with the spatial distribution of the lasing mode, in spite of both distributions being obtained by means of the different approaches (FDTD and Monte Carlo techniques).

patterns. They are characterized by the presence of "hot spots" of typical submicron sizes. We note that such patterns are a generic near-field imaging feature for various 2D systems near percolation [33,34].

Figures 6(a)–6(c) display the complete FDTD simulations of the 3D spatial structure of the field amplitude E_x generated by emitters incorporated in a percolating cluster at different times after the pumping start. Initially, before the lasing start time $t_s = 4$ ps, the emission appears from small-scaled uncoupled domains which give rise to weak incoherent radiation with random phases; see Fig. 6(a). Subsequently, however, radiation from the nearest patterns is being synchronized that leads to the formation of macroscopically large areas (patterns) of field.

In every cluster the partial lasing state will be established and this leads to an overall increase of coherent emission. For longer times, the other behavior of the field is observed. From Fig. 6(b) one can see that the lasing modes are confined to 3D areas around the localization centers. Each mode has its own specific frequency and corresponds to a peak in the radiated spectrum inside the system (see Fig. 3). From Fig. 6(b) we observe the random field structure where the coupled coherent field patterns have arisen.

As a result of nonlinear dynamical evolution, the areas with strong field are extended due to the merging of small-scaled structures and reconnecting of the field patterns. A coherent lasing occurs in this percolating system. Once the lasing has started, the gain no longer depends on the pumping rate but is controlled by the losses in the system. From Fig. 6(c) we observe that the field is concentrated in a number of 3D spatially interconnected spots which mainly are located in the central part of the percolating medium.

One can see from Figs. 6(a)–6(c) that all optical 3D modes are strongly mixed and it is difficult to separate a dominated mode among others. To get insight into the structure of the lasing mode, in the next section we will apply the Fermat variation principle that allows us to find the interconnecting trajectories between the emitters.

IV. SPATIAL DISTRIBUTION OF THE FIELD EMITTERS

In this section we study how the optical communications between the emitters establish the field correlations and collective interactions in the inhomogeneous distributed nanostructures. Also the spatial structure of the localized laser modes is discussed. The structure can be composed by optical emitters, quantum dots, or other light emitting objects; see Refs. [3,4] and references therein. No analytical solution is known for the field mode in the considered 3D percolating nonlinear system, and numerical methods have to be used. We start from the simple approach allowing to obtain the "geometrical" characteristics or trajectory of such mode in the geometrical optics approximation.

As we observe from Fig. 6(c) corresponding to the advanced laser generation, the lasing mode acquires a complicated 3D spatial structure, different from the geometry of the emitter distribution. The dominant lasing mode joins all the emitters and results in rapid phase synchronization. Such a mode can be imagined as a trajectory that passes once on each emitter and it does not have closed small-scale loops. This dominant trajectory possesses the optimal path (the minimum spatial length in our case) in comparison to other modes.

In general, the definition of this optimal path is an advanced problem for the structures with a large number of randomly placed emitters. The well-known principle of Fermat [35] asserts that the optimal optical path S between any two points $\mathbf{r}_0$ and $\mathbf{r}_1$ is defined by minimization of

$$S = \int_{r_0}^{r_1} n_r ds = \min , \tag{4}$$

where n_r is the refractive index of the media. For such a variational problem different approaches have been offered. We refer here the traveling salesman problem (TSP) as one of the best studied optimization approaches [36]. The TSP is to find the shortest path starting from an initial point r_0, visiting a given number of points, and ending in the point r_1. The path S obviously depends on the order in which the emitters are visited. Here we apply the TSP approach based on the adaptive simulated annealing algorithm [36] to search for the minimal optical path S joining the emitters integrated in a percolating spanning cluster.

Figure 1 shows the light emitters incorporated in the cluster ordered by the Fermat principle with applying the Monte Carlo technique. The definition of the optimal optical path S, that defines the dominate lasing mode, leads to the ordination of nearest-neighbor emitters and allows studying of the general collective properties of field. Indeed, such a TSP trajectory visits and synchronizes all the emitters and therefore corresponds to a closed dominant mode. Because of the condition to visit all the emitters, the leakage from the system is suppressed and this mode has the largest semiclassical lifetime. The emitters coupled in this way trap the light and produce the lasing effects.

To obtain more support to the semiclassical calculation using the Fermat principle and to get additional insight into

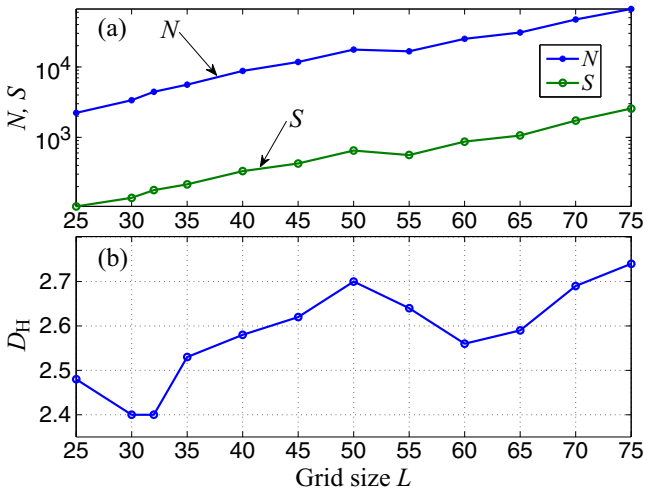

FIG. 8. (Color online) The structure of the percolating cluster as function of the system size (the numerical grid L in FDTD simulations) at the probability population of percolating cluster near $p_c \approx 0.325$. (a) Number of emitters in a percolating cluster N and the length of Fermat optimal path S; see Eq. 4. (b) The fractal (Hausdorff) dimension D_H of the path S. The standard deviation $\sigma \approx N^{-1/2}$ for N in panel (a) is less than 10^{-2}.

the structure of the lasing mode, we have performed a complete long-time ($t \gg t_s$) FDTD simulation to study the result of laser mode competition. The latter allows studying the formation of the laser field structure having longest lifetime. The other modes are dynamically decayed due to the leakage out of the system. After that we can compare the spatial distribution of found dominant lasing mode with the Fermat optical path. Figure 7 shows the result of this long-time FDTD simulation performed for the same parameters as in Fig. 1. From a comparison of Figs. 7 and 1 we observe that, surprisingly, both distributions show reasonably good correlations, despite that they have been calculated on the basis of very different frameworks (FDTD and Monte Carlo). This justifies the usability of the Fermat trajectory approach to study the lasing in percolating structures.

To quantify the characteristic spacial features of lasing field E shown in Fig. 7 we calculate the inverse participation ratio defined as

$$I = \frac{l_0^3 \int |\mathbf{E}|^4 d^3r}{(\int |\mathbf{E}|^2 d^3r)^2} = \left(\frac{l_0}{\xi}\right)^3. \quad (5)$$

While this quantity does not reflect the essential anisotropy of the lasing mode seen in Fig. 7, it allows us to estimate the typical size of the mode ξ. For the percolating cluster with concentration $p_c = 0.32$ we obtain $\xi/l_0 = 0.71$, which indicates the extension of the mode over a great part of the system volume. This parameter is an increasing function of the concentration of the light emitting cluster. In particular, we have found that $\xi/l_0 = 0.67$ for $p = 0.2$, $\xi/l_0 = 0.72$ for $p = 0.35$, and $\xi/l_0 = 0.77$ for $p = 0.8$.

Figure 8 shows the number of emitters N and the length of the Fermat optimal path S [panel (a)] and the fractal (Hausdorff) dimension D_H [panel (b)] as a function of the system size (numerical grid L in FDTD simulations) at the probability population of a percolating cluster slightly above the percolation threshold. We observe that while both the number of emitters N in the cluster and the path S grow exponentially with the system size, the fractal dimension D_H of the Fermat path S weakly depends on L. Notably, it has a value close to the well-known fractal dimension of the incipient percolating cluster $D_H \approx 2.52$ [23,24,31]. To calculate D_H the box counting approach [37] elaborated for our purposes [38] has been used.

The complicated shape of the optical path S leads to considerable interference of field waves in the system shown in Fig. 1. Owing to random interferences, multiple-scattering processes will occur in such a percolating medium. At a large number of random emitters the optical Anderson localization can occur as well.

In Fig. 1 the light rays that penetrate the percolating materials are scattered many times in a random fashion before they leave the sample. Such interference in the multiple-scattering process determines the mode structure of the laser shown in Fig. 7. This process takes place without an optical cavity and can therefore occur even in completely transparent active materials where rays propagate freely. Thus, in a disordered percolating system, the effect of the scattering enhances the length of the light paths before photons escape from the system. As a result, the stimulated emission is "improved" by randomness as compared to a homogeneous active medium.

We note that lasing in the percolating system appears due to the joint action of two factors: multiple scattering of emitted light and the gain inside the percolating cluster. Both these effects have a strong random component in the 3D system. We have found that for the samples of small size (tens of microns), the coherent lasing is well established (synchronized) and starts typically for the time of about tens of picoseconds. In real systems one expects to have strong fluctuations of properties near the percolation threshold. As a result, the lasing start time can be very sensitive to the position inside the large samples and this would complicate the description of lasing from macroscopic percolating systems. In particular, while the lasing mode extends to the whole sample size in our case, we do not know the details of spatial structure of lasing modes in macroscopically sized percolating systems.

V. CONCLUSIONS

We have demonstrated that a 3D percolating cluster filled with light emitters can serve as a lasing structure. The time dynamics and spectra of the lasing output are studied numerically with the finite-difference time-domain method. We have demonstrated that lasing from this system can be originated without an optical cavity and can therefore occur even in transparent active materials. Similarly to random lasers the appearance of coherent emission is related to the substantial increase of the optical path for the escaping radiation. The optimal optical path for communication between the radiated emitters can be found by applying the Fermat principle together with the Monte Carlo approach. The lasing mode is found by a long-time FDTD simulation that allowed studying the formation of spatial field structures in a nonlinear regime. Both FDTD and Monte Carlo approaches reveal reasonably good correlations. We have shown that in distinction to the random lasing structures, the directivity of the percolation

cluster closely to the percolating transition leads to a significant anisotropy of emission from this mirrorless system, with a substantial part of lasing coming out along the direction of percolation.

ACKNOWLEDGMENTS

This work was supported in part by CONACYT (México) under Grant No. 246220.

[1] D. S. Wiersma, M. P. van Albada, and A. Lagendijk, Nature (London) **373**, 203 (1995).
[2] D. S. Wiersma and A. Lagendijk, Phys. Rev. E **54**, 4256 (1996).
[3] L. Wang, S.-J. Zhu, H.-Y. Wang, S.-N. Qu, Y.-L. Zhang, J.-H. Zhang, Q.-D. Chen, H.-L. Xu, W. Han, B. Yang, and H.-B. Sun, ACS Nano **8**, 2541 (2014).
[4] X. Wen, P. Yu, Y.-R. Toh, X. Ma, and J. Tang, Chem. Commun. **50**, 4703 (2014).
[5] V. S. Letokhov, Zh. Eksp. Teor. Fiz. **53**, 1442 (1967) [Sov. Phys. – JETP **26**, 835 (1968)].
[6] H. Cao, Y. G. Zhao, S. T. Ho, E. W. Seelig, Q. H. Wang, and R. P. H. Chang, Phys. Rev. Lett. **82**, 2278 (1999).
[7] S. V. Frolov, Z. V. Vardeny, K. Yoshino, A. Zakhidov, and R. H. Baughman, Phys. Rev. B **59**, R5284 (1999).
[8] N. M. Lawandy, R. M. Balachandran, S. S. Gomers, and E. Sauvain, Nature (London) **368**, 436 (1994).
[9] X. Meng, K. Fujita, S. Murai, and K. Tanaka, Phys. Rev. A **79**, 053817 (2009).
[10] A. K. Tiwari, K. S. Alee, R. Uppu, and S. Mujumdar, Appl. Phys. Lett. **104**, 131112 (2014).
[11] A. Yu. Zyuzin, Phys. Rev. E **51**, 5274 (1995).
[12] S. John and G. Pang, Phys. Rev. A **54**, 3642 (1996).
[13] C. Vanneste, P. Sebbah, and H. Cao, Phys. Rev. Lett. **98**, 143902 (2007).
[14] R. Uppu and S. Mujumdar, Phys. Rev. A **90**, 025801 (2014).
[15] D. S. Wiersma, Nat. Phys. **4**, 359 (2008).
[16] S. John, Phys. Rev. Lett. **53**, 2169 (1984).
[17] P. W. Anderson, Philos. Mag. B **52**, 505 (1985).
[18] A. Lagendijk, M. P. van Albada, and M. van der Mark, Physica A **140**, 183 (1986).
[19] C. Conti and A. Fratalocchi, Nat. Phys. **4**, 794 (2008).
[20] G. Burlak, A. Diaz-de-Anda, Yu. Karlovich, and A. B. Klimov, Phys. Lett. A **373**, 1492 (2009).
[21] G. Burlak, M. Vlasova, P. A. Marquez Aguilar, and L. Xixitla-Cheron, Opt. Commun. **282**, 2850 (2009).
[22] G. Burlak and Y. Calderon-Segura, Physica B **453**, 8 (2014).
[23] M. B. Isichenko, Rev. Mod. Phys. **64**, 961 (1992).
[24] D. Stauffer and A. Aharony, *Introduction to Percolation Theory*, 2nd ed. (CRC, Boca Raton, 1992).
[25] M. A. Noginov, J. Novak, D. Grigsby, and L. Deych, J. Opt. A: Pure Appl. Opt. **8**, S285 (2006).
[26] A. E. Siegman, *Lasers* (University Science Books, Mill Valley, CA, 1986).
[27] X. Jiang and C. M. Soukoulis, Phys. Rev. Lett. **85**, 70 (2000).
[28] M. Sargent III, M. O. Scully, and W. E. Lamb, Jr., *Laser Physics* (Addison-Wesley, Reading, MA, 1974).
[29] A. Taflove and S. C. Hagness, *Computational Electrodynamics: The Finite-Difference Time-Domain Method*, 3rd ed. (Artech House, Norwood, MA, 2005).
[30] J. Sanghera, W. Kim, G. Villalobos, B. Shaw, C. Baker, J. Frantz, B. Sadowski, and I. Aggarwal, Materials **5**, 258 (2012).
[31] J. Wang, Z. Zhou, W. Zhang, T. M. Garoni, and Y. Deng, Phys. Rev. E **87**, 052107 (2013).
[32] D. Meschede, *Optics, Light and Lasers* (Wiley-VCH, New York, 2007).
[33] A. K. Sarychev and V. M. Shalaev, Phys. Rep. **335**, 275 (2000).
[34] W. J. M. Kort-Kamp, P. I. Caneda, F. S. S. Rosa, and F. A. Pinheiro, Phys. Rev. B **90**, 140202 (2014).
[35] M. Born and E. Wolf, *Principles of Optics*, 7th ed. (Pergamon, New York, 1980).
[36] W. H. Press, S. A. Teukovsky, W. T. Vetterling, and B. P. Flannery, *Numerical Recipes in* C++ (Cambridge University Press, Cambridge, England, 2002).
[37] L. Liebovitch and T. Toth, Phys. Lett. **A141**, 386 (1989); J. Sarraille and L. Myers, Educ. Psychol. Meas. **54**, 94 (1994).
[38] G. Burlak and A. Diaz-de-Anda, Opt. Commun. **281**, 181 (2008).